FRACTAL STRUCTURES IN $PbF_2/Pb(NO_3)_2$ PRECIPITATE SYSTEMS

Lara MANDALIAN[1] and Rabih SULTAN[2,*]

Department of Chemistry, American University of Beirut, Beirut, Lebanon;
e-mail: [1] laroshka77@hotmail.com, [2] rsultan@aub.edu.lb

Received June 24, 2002
Accepted November 12, 2002

Tree-like aggregates (dendrites) have been reported in a variety of precipitate systems. We here explore different routes for the growth of dendrites of PbF_2 and $Pb(NO_3)_2$. The PbF_2 ramifications form *via* the interdiffusion of coprecipitates (F^- into Pb^{2+}) in microslides (Liesegang-type experiments) and *via* the infiltration of electrolyte through cracks, thus simulating geochemical fractals. The $Pb(NO_3)_2$ dendrites are grown by evaporation of dilute solutions of the salt. Images of the various patterns obtained are analyzed and their fractal dimensions are determined. The location of the edges of successive "cascades" in dendritic patterns obeys a spacing law similar to that of Liesegang bands.
Keywords: Liesegang; Periodic precipitation; Fractals; Dendrites; Infiltration; Lead; Fluorides; Crystallizations.

In an earlier paper[1], we explored the various crystalline shapes found in periodic precipitation systems. Exotic crystal morphologies characterize a wide class of precipitate patterns in gelled media. Uniform precipitation fronts[2], Liesegang bands[3,4] and speckled patterns[1] mostly appear in systems where a gel region containing a specific ion is invaded by a solution of its coprecipitate. Although the precipitate domains in such systems may consist of thick, compact bands, they sometimes are distinctly made up of isolated particles of characteristic crystalline shape. Examples of selected crystals include spots, needles, crystallites and notably dendrites, of fractal nature. Dendrites are tree-like aggregates with complex branching and ramification manifested on widely different length scales. Fractal dendritic structures can be found in a variety of natural and biological systems such as trees, snow flakes, dry soil cracks, bacteria colonies and networks of nerves, blood vessels and lung tubes[5,6]. In chemical systems, dendrite formation is mostly observed in precipitation[7–10] and electrodeposition of metals[11–14]. In geology, dendrites and branched structures characterize the growth of certain minerals (such as manganese oxide) in rocks[15,16]. Theoretically, the dynamics in colloidal aggregates was simulated by the diffu-

sion-limited aggregation (DLA) model[17,6]. The computer simulations yield chain structures with tree-like ramifications, much resembling the aforementioned branching systems. An elaborate reaction-diffusion-aggregation model was proposed by Chopard *et al.*[16] as a simple mechanism for the precipitation and growth of mineral dendrites. Büki *et al.*[9] obtained dendrites by simulation of a diffusion-supersaturation model where probabilistic nucleation was induced by random concentration fluctuations. Bacterial colony aggregates display various branching patterns[5], ranging from DLA-like to dense branching morphology (DBM) structures[18].

Fractal objects are mostly characterized by their "fractal dimension" D, a non-integer number lying between the topological dimension (D_T) and the embedded dimension (E) of the object[19]. Typically, for a two-dimensional surface, the embedded dimension is 2 and thus $1 < D < 2$. While mathematical fractals[20,21] are generated by a *deterministic rule*, physical fractals are more or less random with no high level of symmetry[6]. Yet, the latter resemble deterministic fractals in their dilation properties just like stochastic mathematical fractals resemble their symmetric analogs, and are *self-similar* in a statistical sense[19,6].

In a previous paper[1], we reported a set of experiments on PbF_2 precipitation in agar gel whose original aim was to study the Liesegang band formation in this system. We observed two main categories of phenomena depending on which is the diffusing electrolyte (*i.e.* Pb^{2+} or F^-) and which electrolyte is in the gel. With Pb^{2+} above and F^- below (in a vertical tube), distinct Liesegang bands were obtained at all concentration ranges. When the roles of the coprecipitates were reversed (Pb^{2+} in the gel, F^- diffusing), a variety of patterns displaying different crystal shapes, notably spots and dendrites was obtained in the total absence of Liesegang bands. It was especially interesting to observe a network of dendritic structures even in thin tubes of 5.0 mm diameter, shown in Fig. 1a.

Because of the richness of such structures, the experiments were repeated in microslides for a more convenient observation under microscope. Macroscopic pattern of a sample grown in a gel sandwiched between two microslides (in a Liesegang-type experiment) is shown in Fig. 1b.

In the present paper, we focus on the development of various experimental methods for preparing dendritic precipitate patterns with a testing of their reproducibility, along with their characterization from the viewpoint of fractal growth. The aims of the study may thus be summarized as follows:

1. Reporting a set of experiments that describe different routes for obtaining precipitate patterns with dendritic networks. One route notably pro-

vides an interesting analogy with geological infiltration of mineral-rich water in a rock fissure or crack[15].

2. Characterizing those dendrites by calculating the fractal dimension using the box-count method[22] (see Results and Discussion). The calculations will be performed on scanned images of the various patterns taken on a microscopic level.

EXPERIMENTAL

Routes for Precipitate Dendrites

We present here a set of precipitate patterning experiments where dendrite structures are obtained. Three main routes for the growth of dendritic crystals are described: interdiffusion (Liesegang-type procedure), infiltration and evaporation.

Interdiffusion (Classic Liesegang) Experiments

Two glass microslides with a spacer of thickness 2.5 mm were sealed with silicone except from the top (*i.e.* leaving one end open). A gel solution was prepared by boiling a solution that is 1% in agar and contains $Pb(NO_3)_2$ of variable concentrations (0.20–0.50 M). The hot solution was poured into the inter-slide cavity and allowed to cool. After the gel solidified, a 1.0 M KF solution was poured on the top of the gel and sealed with silicone to prevent evaporation. A dense zone of PbF_2 precipitate was first observed. After a long time (around 35 days), a pattern of branching PbF_2 dendrites appeared and spread over the whole area in the course of several days. We refer to this procedure as one of the Liesegang type, because the procedure is similar in that a solution of a given ion is allowed to diffuse into a gel solu-

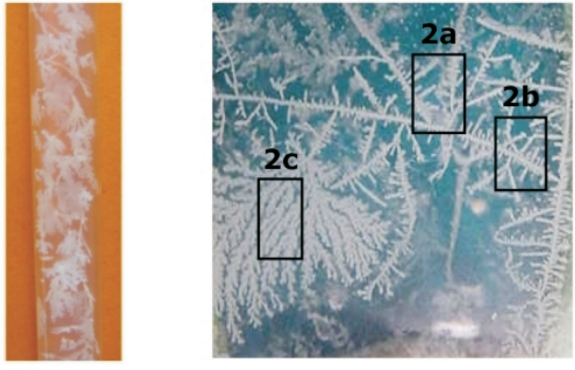

FIG. 1
Dendrites of PbF_2 grown in tubes (a) and in glass microslides (b). In both cases, a solution of F^- ions diffuses into an agar gel containing Pb^{2+}. $[F^-]_0$ = 1.0 M, $[Pb^{2+}]_0$ = 0.4 M. Gel medium thickness 2.5 mm; gel width 1.7 cm. The black frames in b correspond to those of Fig. 2, shown there while magnified and photographed under microscope (see Fig. 2)

tion of its coprecipitate. Note, however, that no Liesegang bands were obtained except when the roles of the electrolyte solutions were inverted[1]. The concentration ranges that actually give dendrites were chosen as directed in ref.[1], where the various domains yielding different types of crystal structures were determined. Figure 1a shows dendritic flakes in a tube; while Fig. 1b displays a typical network of branched dendrites grown between glass microslides. Frames a–d of Fig. 2 display photomicrographs of regions of the same pattern (as the one in Fig. 1b) at various selected locations. Image analysis of those pictures is presented in Results and Discussion. Another set of experiments was performed between methacrylate glass microslides separated by 1.5 mm spacers. The width of the gel surface was decreased to induce a more directional character of the dendrites. Exactly the same procedure was followed, but here elongated cascades of branched structures of a less random nature were consistently observed, evolving gradually downwards. The time sequence after the onset of first ramifications is displayed in Fig. 3. The dendrites emerging from the bottom after 41 days may be attributed to a state of supersaturation with no initiation of nucleation, resulting in a zone void of precipitate. After diffusion has reached the bottom, nucleation was apparently initiated and the growing dendrites continued to fill the gap zone (see image at 42 days). Due to the slight opaqueness of the organic glass and the small size of the constituent images, Fig. 3 lacks clarity here, and a magnification is provided on the web at the link: http://staff.aub.edu.lb/~rsultan/Images/Fig3.jpg. The edges of consecutive cascades in the pattern seemed to satisfy the spacing law observed in Liesegang bands. The locations (x_n) were determined at the edge of each cascade right after its completion, and are depicted in Fig. 4.

Note that the edges are easy to locate because there is a time lag between two successive cascades as can be inferred from the time sequence of Fig. 3. The edge locations (relative to the interface between the gel and the outer solution, denoted x_n) along with the spacing ratios $\rho_n = x_{n+1}/x_n$ are given in Table I.

We can see that the spacing ratio (which is always >1) decreases slightly as the number n increases just like in a banded Liesegang pattern. A similar observation on the spacing law in cascades of dendrites was reported by Zrínyi *et al.*[9] in PbI_2 experiments. Figure 5 shows

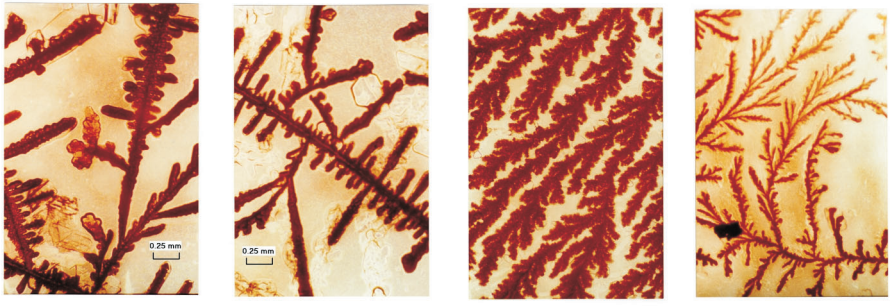

FIG. 2

Photomicrographs of the PbF_2 dendrites obtained between microslides, shown in Fig. 1b. The first three (frames a, b and c) correspond to the regions in the black frames of Fig. 1b. The pattern in frame d is not shown in the macroscopic picture. The fractal dimensions corresponding to these patterns were calculated and recorded in Table II

TABLE I
Locations of cascade edges (x_n) and spacing ratios (ρ_n) in the dendrite pattern of Figs 3 and 4

n	x_n, cm	ρ_n
1	1.28	–
2	2.04	1.59
3	2.91	1.43
4	4.05	1.39

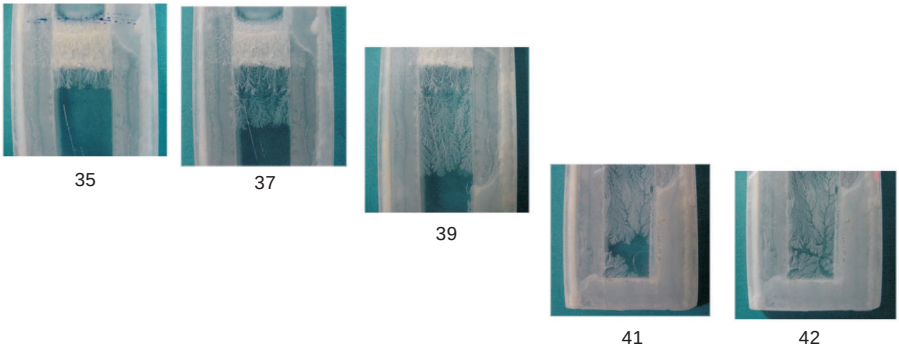

FIG. 3
Time sequence of the growth of dendrites in methacrylate glass slildes with gel thickness of 1.5 mm; gel width 0.9 cm. The time (in days) is shown under each picture. $[F^-]_0$ = 1.0 M, $[Pb^{2+}]_0$ = 0.3 M. Unlike the random dendrites of Fig. 2, the pattern here appears as directional cascades whose edges stop at specific time steps

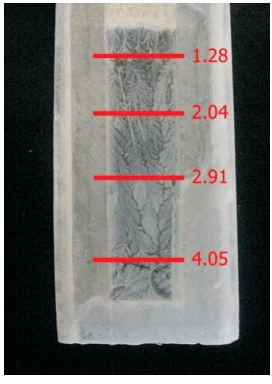

FIG. 4
The same pattern as in Fig. 3 with positions of the edges of successive cascades, measured (in cm) from the interface between the gel and the diffusing solution. The spacing ratio seems to agree with that observed in Liesegang banding systems (see Table I)

portions of the dendritic patterns of Fig. 4 observed under microscope. Fractal characteristics of those cascades are considered in Results and Discussion.

Infiltration Experiments

In this section, we report some experiments in which PbF_2 dendrites are formed in a way similar to the growth of crystals in minerals, in the cracks and fissures of rocks. The procedure was similar to that described briefly in ref.[15] Two glass plates (7 × 7 cm) were maintained at a 1.0 mm distance (using a spacer) and sealed with silicone leaving only one side open. A hot gel solution of Pb^{2+} (1% agar and 0.45 M $Pb(NO_3)_2$) was then poured into the thin space between the plates with care not to allow any air bubble formation. The solution was left to cool until gelation is complete, after which the open end of the cavity was sealed with silicone. We thus had a thin square layer of lead nitrate gel sandwiched between two glass plates sealed from all sides, and hence easy to manipulate. This "sealed square dish" was immersed in a 1.0 M KF solution contained in a large vessel. Afterwards, while inside the solution, the dish was struck with a hammer causing a set of fractures across the glass of its top plate. Those fractures could to a certain extent simulate the cracks that occur in a rock covered with drainage waters rich in dissolved minerals. After a time lag of 51 days (measured consistently in two samples) during which no precipitation was detected, random

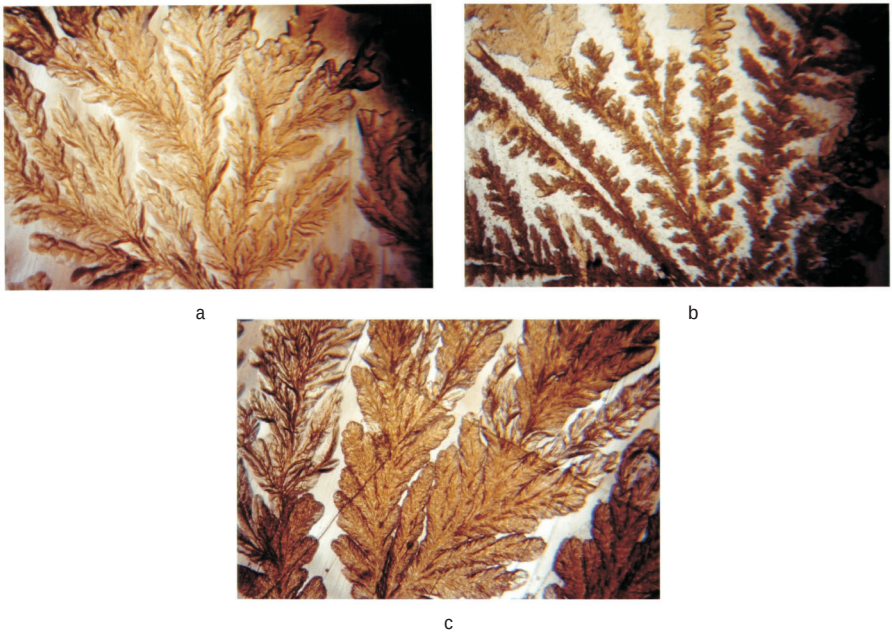

FIG. 5
Photomicrographs of spatial portions of the dendrite cascades in Figs 3 and 4. The fractal dimension of each portion is reported in Table II

PbF_2 crystallites started to appear along the cracks, then continued to form along the pathway of fractures, but not linked in a network like the dendrites grown in the microslide Liesegang experiments. Figure 6 highlights pictures of various crack zones illustrating the initiation of the PbF_2 crystallites on both sides of the fracture. The time evolution of the pattern spreading, originating at the cracks then invading the whole area, is seen in Fig. 7. Figure 8 highlights areas of the pattern from Fig. 7 photographed under microscope.

Evaporation

A very interesting network of dendritic structures was discovered when $Pb(NO_3)_2$ crystals were grown from a solution by evaporation. These exotic patterns warrant a further investigation. A number of experiments was subsequently performed by evaporating the solvent from a gel layer containing $Pb(NO_3)_2$ at different concentrations (0.10, 0.30 and 0.50 M). In order to maintain a uniform thickness of the gel layer (1.5 mm), the same volume (10.0 ml) of gel solution was poured in dishes of similar geometry. The resulting macroscopic texture of dendritic patterns, observed after evaporation, is shown in Fig. 9. Figure 10 displays photomicrographs of selected regions of the patterns obtained by evaporation (the 0.50 M case).

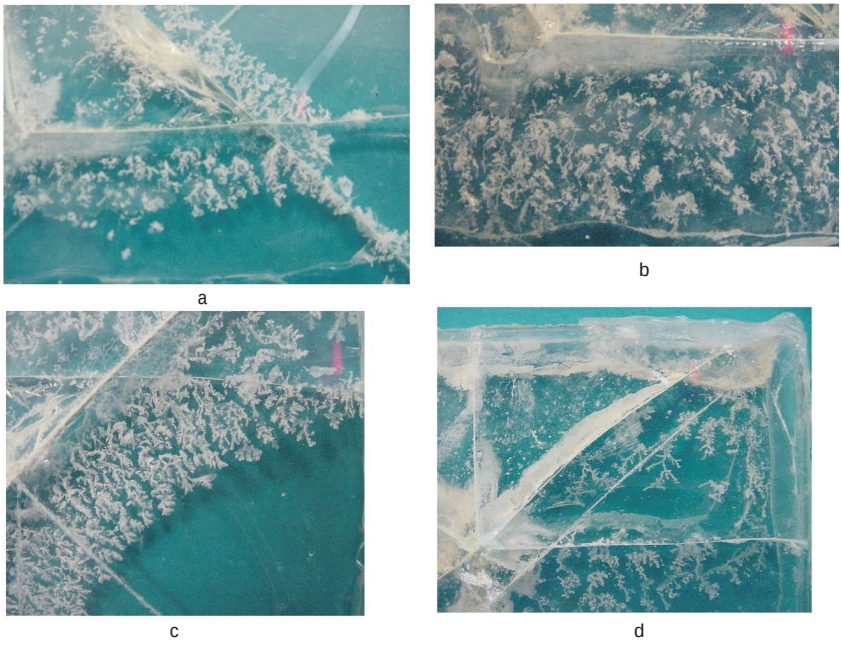

FIG. 6
PbF_2 dendrites obtained form crack infiltration experiments described in Experimental (Infiltration Experiments). A solution with $[F^-]_0$ = 1.0 M infiltrated and diffused through cracks caused by hammering into a gel solution with $[Pb^{2+}]_0$ = 0.45 M. The different frames show different crack regions where the dendrite formation originates

RESULTS AND DISCUSSION

Characterization and Discussion

Physical processes never lead to structures with perfect symmetry[6]. Geometric constructions constitute idealized structures for demonstrating the calculation of exact fractal dimensions[22]. Such structures are highly symmetric when built in a consistent reproduction of patterns and are termed, in that case, *deterministic* fractals[6]. Structures having exactly the same fractal dimension, though without having the same visual appearance, are called *stochastic* fractals. Physical processes are always subject to fluctuations and thus lead to *random* fractals. Image analysis techniques add to small-angle scattering and energy transfer methods in characterizing fractals[19]. The most commonly used image analysis technique is the box-count

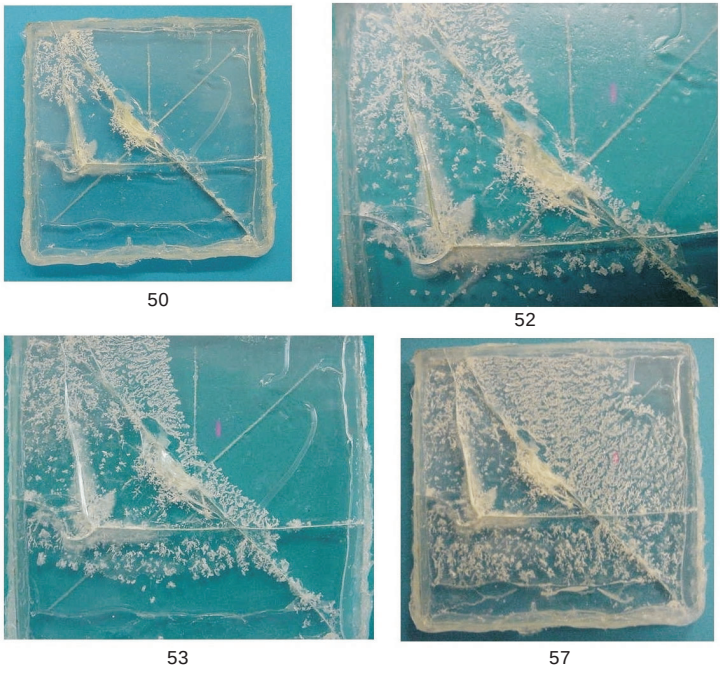

FIG. 7
Time sequence of the infiltration/precipitation process described in Experimental (Infiltration Experiments) and in Fig. 6. The experiment exhibited a delay of 51 days followed by a sudden appearance of dendritic precipitate (PbF_2) structures. The pattern, originating near the crack, spreads gradually over the whole gel area. The time in days is displayed below the picture frames

method[22,19,21]. Given λ, a characteristic lower cut-off for the measuring length scale, we consider a grid of square boxes of side λ. The ramified structure has area $n\lambda^2$, where $n(\lambda)$ is the number of covered cells (boxes). Because the number of boxes $n(\lambda)$ covers a spatial region of fractal dimension D, and because $n(\lambda)$ decreases as λ increases, it follows that $n(\lambda) \approx (1/\lambda)^D$. The box-counting dimension is thus defined by taking the natural logarithm of both sides.

$$D = \frac{\ln n(\lambda)}{\ln(1/\lambda)} \qquad (1)$$

It is obvious that for a non-fractal object, the above definition yields a trivial value for D, namely the embedded Euclidean dimension E. A plot of ln $n(\lambda)$ *versus* ln $(1/\lambda)$ should yield a straight line of slope D, the fractal box-dimension. Though physical fractal objects do not yield consistently the same fractal dimension, the latter nevertheless gives a good measure when all the values calculated for different portions of the same object fall within

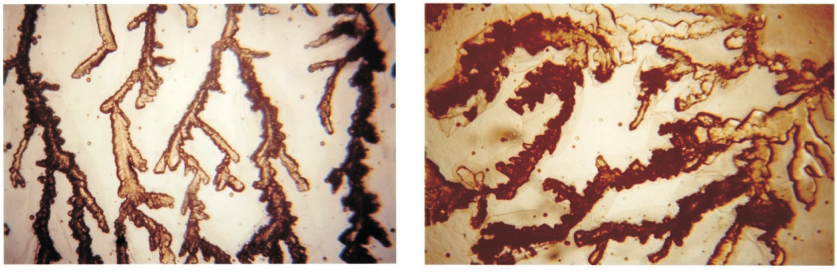

FIG. 8
Photomicrographs of PbF_2 dendritic patterns obtained by infiltration experiments (Figs 6 and 7). The patterns are analyzed in Table II

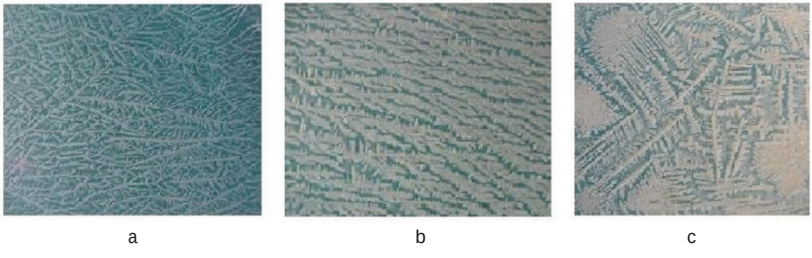

FIG. 9
Network patterns of $Pb(NO_3)_2$ of initial concentration C obtained by evaporation of an agar gel solution of the salt. a C = 0.1 M, b C = 0.3 M, c C = 0.5 M

TABLE II
Fractal dimensions calculated using the box-counting method for the various microstructures illustrated in Figs 2, 5, 8 and 10. *D*, fractal dimension; σ, standard deviation

Plate	Experiment type	Container	*D*	σ
2a	interdiffusion	glass microslides	1.82	0.01
2b	interdiffusion	glass microslides	1.85	0.01
2c	interdiffusion	glass microslides	1.71	0.02
2d	interdiffusion	glass microslides	1.88	0.01
5a	interdiffusion	methacrylate glass microslides	1.82	0.01
5b	interdiffusion	methacrylate glass microslides	1.76	0.01
5c	interdiffusion	methacrylate glass microslides	1.77	0.01
8a	hammering/infiltration	glass plates	1.87	0.004
8b	hammering/infiltration	glass plates	1.86	0.003
10a	evaporation (0.50 M)	Petri dish	1.90	0.003
10b	evaporation (0.50 M)	Petri dish	1.83	0.01
10c	evaporation (0.50 M)	Petri dish	1.82	0.01

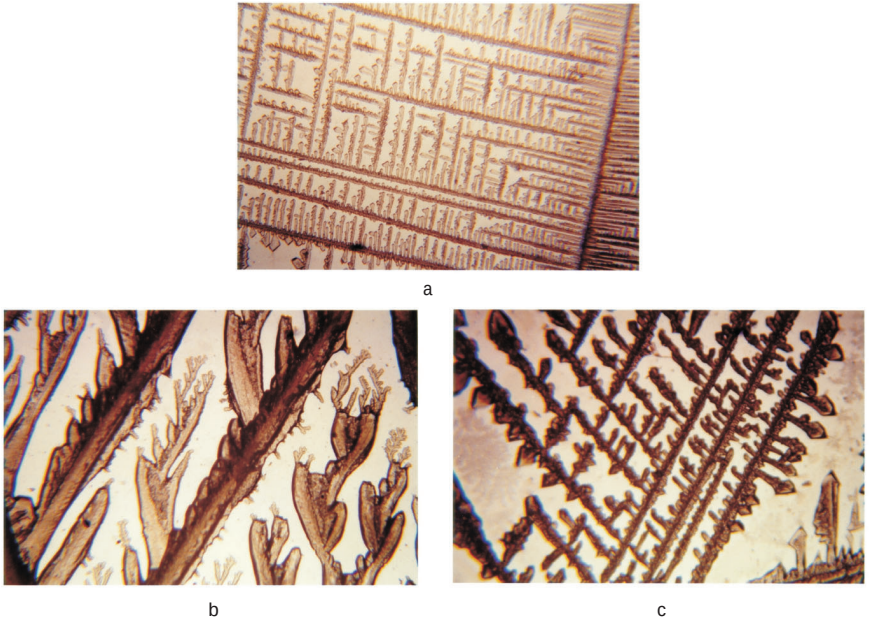

FIG. 10
Photomicrographs of the pattern in Fig. 9c obtained by evaporation. Initial concentration of $Pb(NO_3)_2$ C = 0.5 M. The patterns are analyzed in Table II

a narrow range (≈0.2 for an embedded dimension E = 2.0). Figure 11 highlights such plots for each type of dendritic pattern obtained (*i.e. via* interdiffusion, infiltration or evaporation), corresponding to frames 2b, 8a and

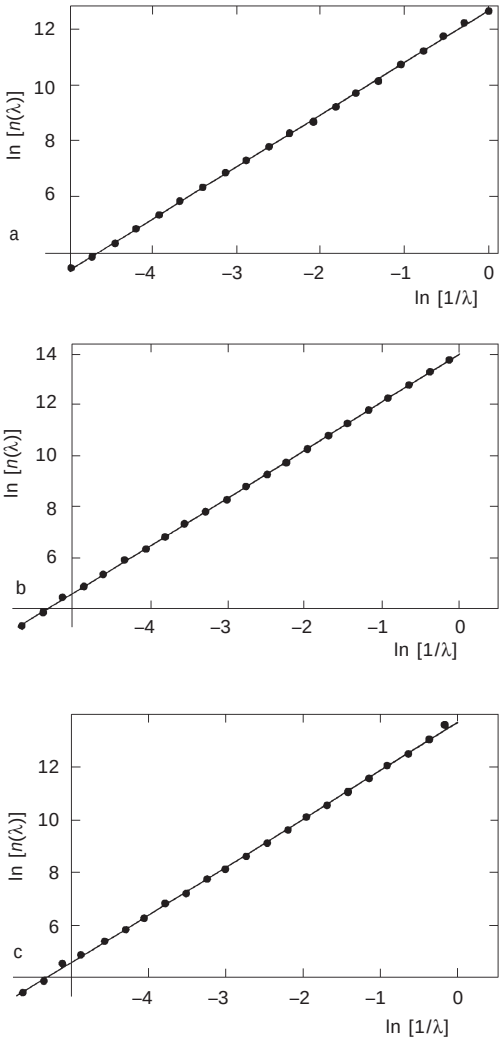

FIG. 11
The ln $n(\lambda)$ versus ln $(1/\lambda)$ plots for the patterns in frames a 2b (interdiffusion), b 8a (infiltration) and c 10b (evaporation), respectively. The plots are linear with slopes equal to the box dimensions D. D = 1.85, 1.87 and 1.83, respectively

10b, respectively. We see that the points fall on a straight line (almost a perfect fit), whose calculated slope yields the fractal dimension *D*.

In Table II, we report values of the box-counting dimension for the photomicrographs of various patterns, computed by image analysis using the Benoît[23] software. The labels in the first column correspond to the plates appearing in various figures. The entries in the second column indicate the type of experiment producing the pattern.

We see that all the values of the fractal dimension in Table II (for PbF_2 dendrites obtained *via any* experimental route and for $Pb(NO_3)_2$ by evaporation), fall within a somewhat narrow range of 0.19. Thus we can say that all the dendritic patterns obtained have essentially a similar fractal box dimension ranging from 1.71 to 1.90, with an average of 1.82 and a mid-range value of 1.81. Because physical fractals are not exactly self-similar, the fractal dimension is often reported over a range of values. A 1.7–1.9 interval was reported for fractal clusters in zinc and iron aerosols[19]. A scatter around the value 1.67 with a 0.11 span was found for 2D zinc radial electrodeposition leaves[11]. Radial viscous fingering patterns obtained in Hele–Shaw cells were shown to be fractal with box dimension in the region 1.75–1.85 [24,25]. The mean value 1.78 was found to characterize hydrous manganese oxide deposits on the surface of Bavarian and Greek limestones, resulting from reaction-diffusion processes[16].

Mimura *et al.*[18] proposed a number of reaction-diffusion models that describe the wide morphological diversity of bacterial growth patterns. The analogy between the latter systems and precipitate patterns, along with the

FIG. 12
Dense branching morphology (DBM) pattern resembling that obtained in bacteria. In the dish: 1% agar gel solution with $[Pb^{2+}]_0$ = 0.30 M, in the tube: $[F^-]_0$ = 0.81 M

parameters controling their formation is under investigation. Interdiffusion experiments (similar to those of Experimental (Interdiffusion Experiments)) performed in a Petri dish wherein the outer solution diffuses radially from a central source yielded interesting dense branching morphology (DBM) structures, shown in Fig. 12.

Networks of irregular macroscopic PbI_2 patterns obtained from initially homogeneous supercooled solutions showed a fractal nature with a lower average dimension of 1.56 [26]. The pattern in the latter systems is described as a two-dimensional network of pores with a characteristic length (and subsequently fractal dimension) which is sensitive to initial concentration.

Thus we see that a rich diversity and complex structure is inherent to precipitate patterning systems and a variety of fractal morphologies can be obtained.

This work was supported by a University Research Board (URB) grant No. DCU17996071617, American University of Beirut.

REFERENCES

1. Panjarian Sh., Sultan R.: *Collect. Czech. Chem. Commun.* **2001**, *66*, 541.
2. Sharbaugh A. H., III, Sharbaugh A. H., Jr.: *J. Chem. Educ.* **1989**, *66*, 589.
3. Liesegang R. E.: *Liesegang's photographisches Archiv* **1896**, *37 (21)*, 321.
4. Henisch H. K.: *Crystals in Gels and Liesegang Rings*. Cambridge University Press, Cambridge 1988.
5. Ball P.: *The Self-Made Tapestry: Pattern Formation in Nature*. Oxford University Press, Oxford 1999.
6. Vicsek T.: *Fractal Growth Phenomena*, 2nd ed. World Scientific, Singapore 1992.
7. Kárpáti-Smidróczki É., Büki A., Zrínyi M.: *Colloid Polym. Sci.* **1995**, *273*, 857.
8. Büki A., Kárpáti-Smidróczki É., Zrínyi M.: *Magy. Kem. Foly.* **1995**, *101*, 524.
9. Büki A., Kárpáti-Smidróczki É., Zrinyi M.: *Physica A (Amsterdam)* **1995**, *220*, 357.
10. Toramaru A., Iochi A.: *Kobutsugaku Zasshi* **1997**, *26*, 103; *Chem. Abstr.* **1997**, *127*, 5521A, 115498b.
11. Matsushita M., Sano M., Hayakawa Y., Honjo H., Sawada Y.: *Phys. Rev. Lett.* **1984**, *53*, 286.
12. Yasugi S., Dougherty A., Gollub J. P.: *Phys. Rev. Lett.* **1986**, *56*, 1260.
13. Grier D., Ben-Jacob E., Clarke R., Sander L. M.: *Phys. Rev. Lett.* **1986**, *56*, 1264.
14. Trigueros P. P., Claret J., Mas F., Sagués F.: *J. Electroanal. Chem.* **1991**, *312*, 219.
15. García-Ruiz J. M., Otálora F., Sanchez-Navas A., Higes-Rolando F. J. in: *Fractals and Dynamic Systems in Geoscience* (J. H. Kruhl, Ed.), p. 307. Springer-Verlag, Berlin 1994.
16. Chopard B., Hermann H. J., Vicsek T.: *Nature* **1991**, *353*, 409.
17. a) Witten T. A., Sander L. M.: *Phys. Rev. Lett.* **1981**, *47*, 1400; b) Witten T. A., Sander L. M.: *Phys. Rev. B: Condens. Matter* **1983**, *27*, 5686.
18. Mimura M., Sakaguchi H., Matsushita M.: *Physica A (Amsterdam)* **2000**, *282*, 283.

19. Harrison A.: *Fractals in Chemistry*, Oxford Chemistry Primers, No. 22. Oxford University Press, Oxford 1995.
20. Barnsley M.: *Fractals Everywhere*. Academic Press, New York 1988.
21. Moon F. C.: *Chaotic and Fractal Dynamics: An Introduction for Applied Scientists and Engineers*. J. Wiley, New York 1992.
22. Mandelbrot B. B.: *The Fractal Geometry of Nature*. Freeman, San Francisco 1982.
23. Mandelbrot B. B.: *Benoit Fractal Analysis System*, Version 1.3. Trusoft, St. Petersburg (FL) 1997–2000.
24. Couder Y. in: *Random Fluctuations and Pattern Growth* (H. E. Stanley and N. Ostrowsky, Eds), p. 75. Kluwer, Dordrecht 1988.
25. May S. E., Maher J. V.: *Phys. Rev. A: At., Mol., Opt. Phys.* **1989**, *40*, 1723.
26. Kai S., Yamada T., Ikuta S., Müller S. C.: *J. Phys. Soc. Jpn.* **1989**, *58*, 3445.